Supplementary Information (SI) for Physical Chemistry Chemical Physics.
This journal is © the Owner Societies 2025

Energy partitioning in H_2 formation on interstellar carbonaceous grains. Insights from *ab initio* molecular dynamics simulations

Supplementary Information

Léana Jubert,[a] Berta Martínez-Bachs,[a] Gerard Pareras,[a] and Albert Rimola[a]

[a] *Departament de Química, Universitat Autònoma de Barcelona, Bellaterra 08193 Catalonia, Spain. E-mail: albert.rimola@uab.cat*

1 Benchmarking

1.1 Gas-Phase Reaction Energy

To assess the accuracy of the computational approach, we benchmarked the reaction energy of H_2 in the gas phase using PBEsol functional employed throughout our AIMD simulations with results from the high-accuracy coupled-cluster method CCSD(T)-F12. The comparison, shown in Table 1, demonstrates the performance of PBEsol relative to this benchmark approach.

Table 1 Benchmark of reaction energies for H_2 in the gas phase under different method

Method	**Reaction Energy (kJ mol^{-1})**
CCSD(T)-F12	−445.5
PBEsol	−450.1

The PBEsol functional yields a reaction energy within 5 kJ mol^{-1} of the CCSD(T)-F12 reference, indicating that it provides a reliable description of the gas-phase energetics for H_2.

1.2 Parameter Testing

To ensure the validity of our results in the surface-adsorbed system, we performed additional benchmarks by varying some computational parameters. These tests were conducted for the PC configuration, which includes both physisorbed and chemisorbed hydrogen, providing a representative case for assessing the accuracy of both interactions. The setup used throughout this study employs a double-ζ (DZ) basis set without short-range (no SR) and a plane-wave cutoff of 500 Ry. We evaluated the impact of using a DZ basis set with short-range (SR), a higher-quality triple-ζ (TZ) basis set, and an increased plane-wave cutoff energy. The corresponding reaction energies for these settings are summarized in Table 2.

Table 2 Reaction energy benchmarks for H_2 in the PC configuration under various computational settings.

Setting	**Reaction Energy (kJ mol^{-1})**
DZ basis (SR), cutoff = 500 Ry	−410.5
DZ basis (no SR), cutoff = 500 Ry (reference)	−356.8
TZ basis (no SR), cutoff = 500 Ry	−353.5
DZ basis (no SR), cutoff = 600 Ry	−356.7

We observe that increasing the basis set to triple-ζ or raising the energy cutoff to 600 Ry results in only minor changes in reaction energy. Therefore, for computational efficiency, we used the DZ basis and an energy cutoff of 500 Ry for calculations. However, the use of a short-range basis set led to significant deviations in the calculated energy release. To ensure an accurate description of the system, we excluded the short-range basis in our study.

2 Evolution of the instantaneous and averaged kinetic energy terms over 2 ps

Figures S1, S2, and S3 display the instantaneous kinetic energy terms and moving average of both H_2 and the graphene surface over the entire 2 ps of the simulation. We observe H_2 formation accompanied by an increase in the kinetic energy of H_2. The magnitude of this increase aligns with the reaction energy of H_2 formation from each initial position. It corresponds to the energy released during the H–H bond formation with the magnitude of the release depending on the initial position of the H atoms. This variation arises from the differences in the adsorption sites and the nature of the interactions between the H atoms and the graphene surface. That is, chemisorbed initial positions, like CC, are characterized by the presence of strong H-–C bonds, which result in reduced energy release, while in contrast, physisorbed initial positions, like PP, show larger exoergic behaviors due to the weaker interactions with the surface. Following H_2 formation, the graphene's kinetic energy increases, while the oscillations in the kinetic energy of the H_2 molecule decrease. This behavior indicates an energy transfer from H_2 to the graphene surface.

Additionally, the sudden drops observed are attributed to the interactions of the chemically desorbed H_2 molecule with the above-placed slab replicas. This is clearly an artifact of the simulations and, for these cases, we rule out the trajectory data points that follow these drops in the numerical analysis, as they do not accurately reflect the true behavior of the processes.

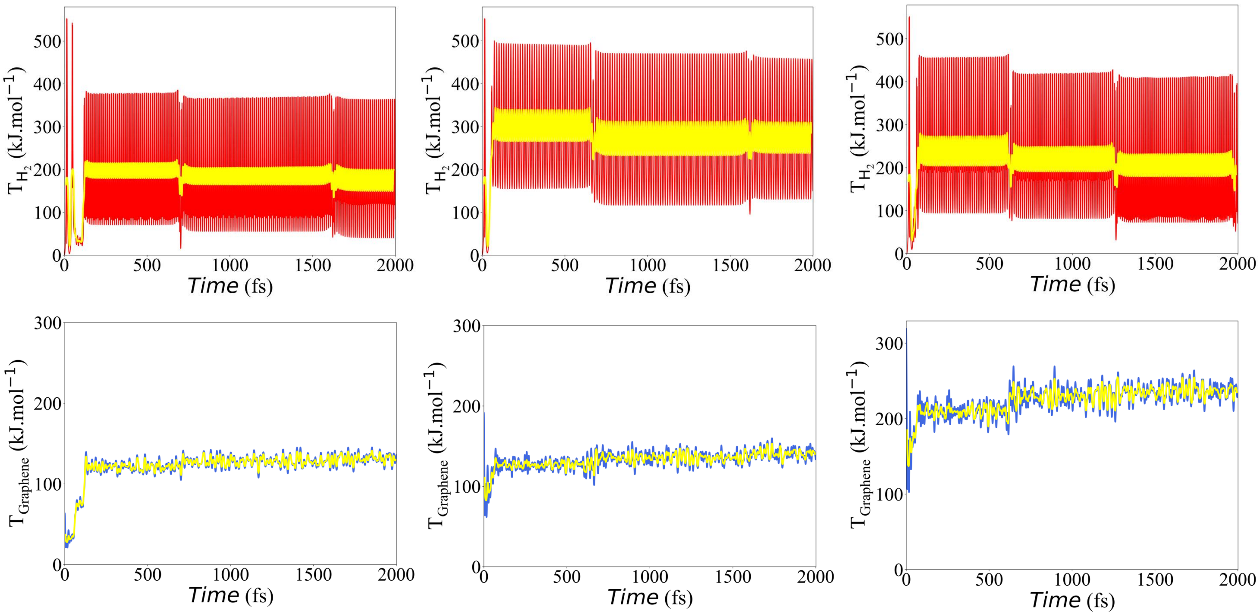

(a) PP at 10K

(b) PP at 30K

(c) PP at 50K

Fig. S1 The top panel shows the evolution of the instantaneous T_{H_2} over time (in red) with its moving average (in yellow) in kJ mol^{-1} for the PP structure at different temperatures. The bottom panel presents the corresponding evolution of the instantaneous $T_{Graphene}$ over time (in blue) along with its moving average (in yellow), in kJ mol^{-1}, for the PP structure at different temperatures.

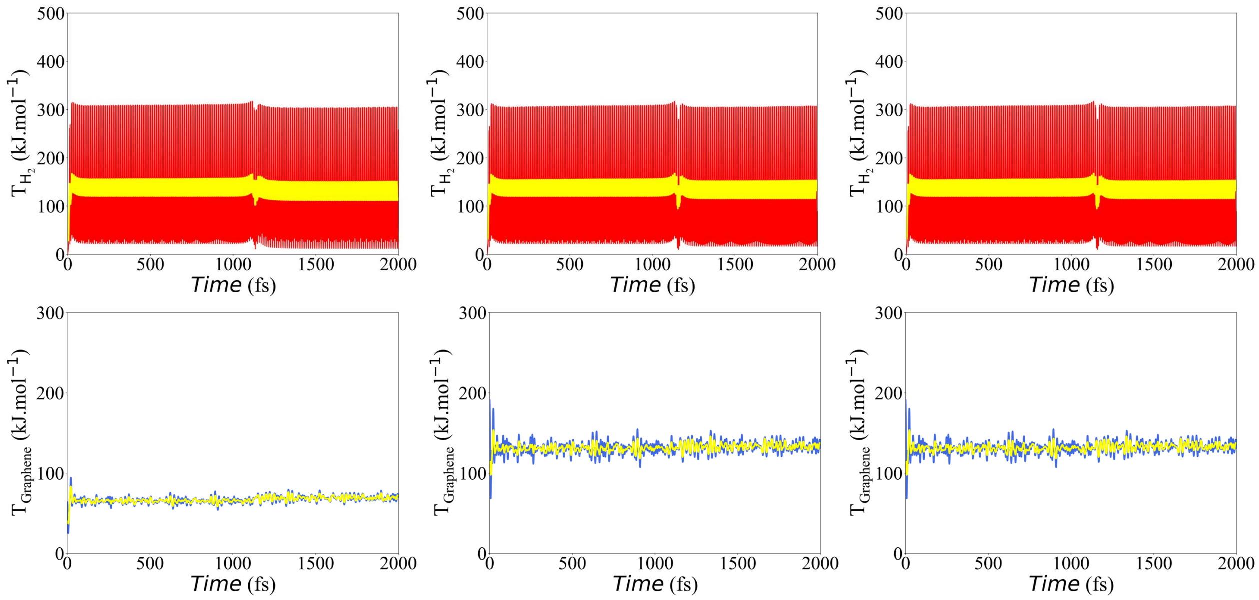

(d) PC at 10K (e) PC at 30K (f) PC at 50K

Fig. S2 The top panel shows the evolution of the instantaneous T_{H_2} over time (in red) with its moving average (in yellow) in kJ mol^{-1} for the PC structure at different temperatures. The bottom panel presents the corresponding evolution of the instantaneous $T_{Graphene}$ over time (in blue) along with its moving average (in yellow), in kJ mol^{-1}, for the PC structure at different temperatures.

3 Distribution in different direction for T_{H_2} over time

Although there is no ambiguity regarding H_2 desorption since the trans-T_z significantly exceeds the binding energy. The plots in Figure S4 reveal how trans-T is partitioned among the three spatial directions. This directional energy distribution helps explain the desorption dynamics: in the CC configuration, most of the translational energy is along the z-axis, so H_2 desorbs perpendicular to the surface. In contrast, in the PC configuration, a larger portion of the energy is distributed along the x and y axes, causing the molecule to desorb more sideways, rather than perpendicular to the surface.

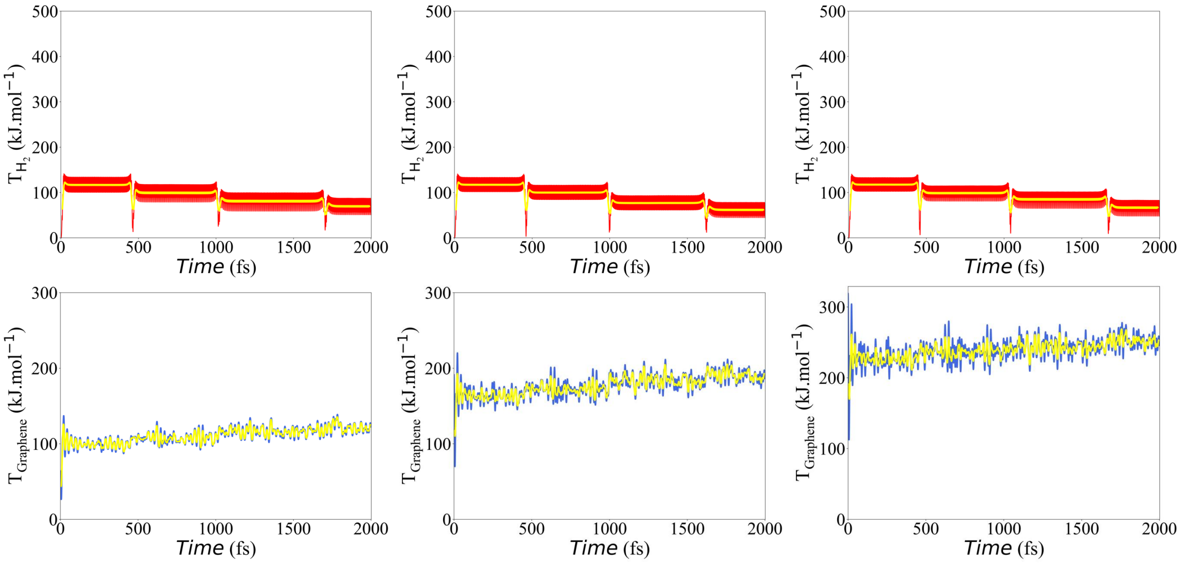

(g) CC at 10K (h) CC at 30K (i) CC at 50K

Fig. S3 The top panel shows the evolution of the instantaneous T_{H_2} over time (in red) with its moving average (in yellow) in kJ mol^{-1} for the CC structure at different temperatures. The bottom panel presents the corresponding evolution of the instantaneous $T_{Graphene}$ over time (in blue) along with its moving average (in yellow), in kJ mol^{-1}, for the CC structure at different temperatures.

4 Evolution of the $T_{graphene}$ in concentric shells for PC and CC

This section presents the evolution of $T_{graphene}$ in concentric shells for the trajectories starting from the PC (Figure S5) and CC (Figure S6) structures.

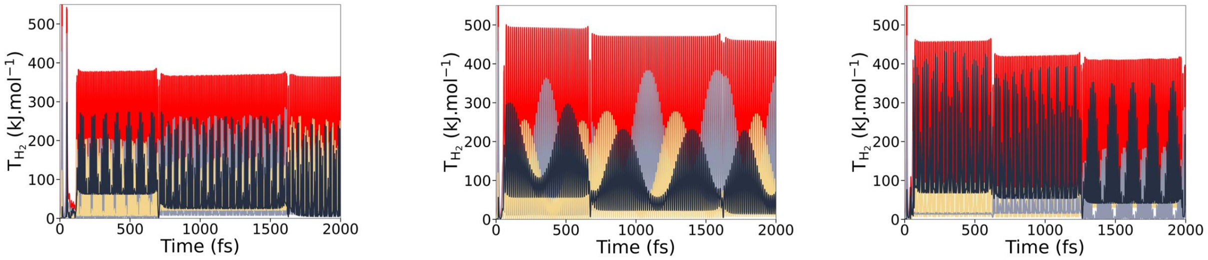

(a) PP at 10K (b) PP at 30K (c) PP at 50K

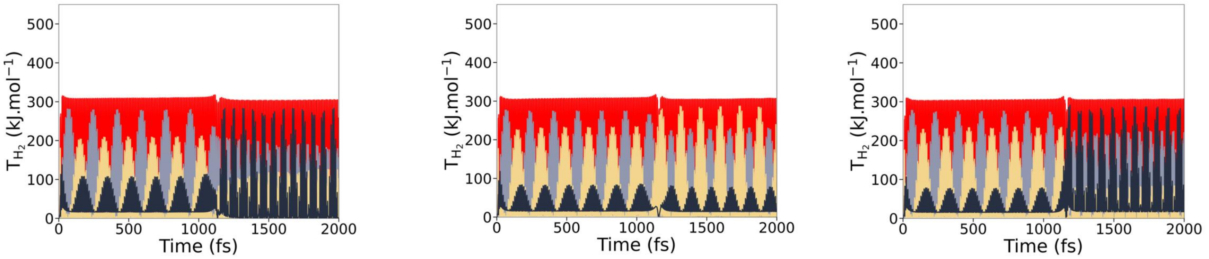

(d) PC at 10K (e) PC at 30K (f) PC at 50K

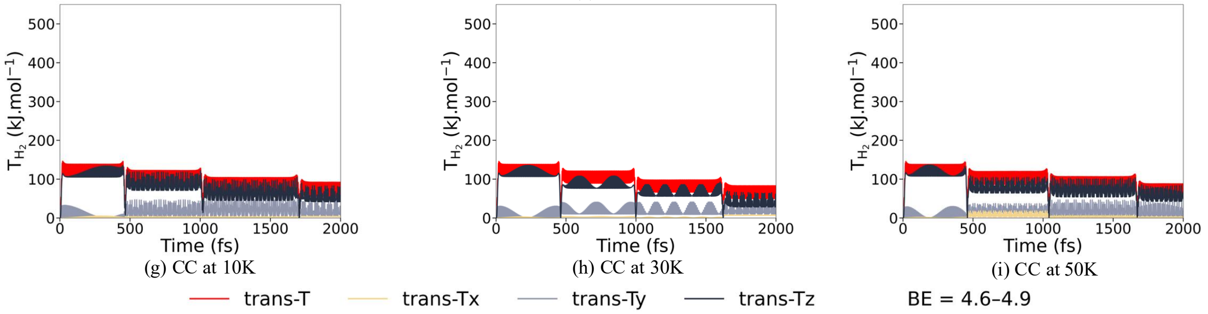

Fig. S4 Evolution of the instantaneous T_{H_2}(trans-T) over time (in red) in kJ mol^{-1} along with its directional components: trans-Tx (in yellow), trans-Ty (in grey), and trans-Tz (in black)

5 H–H bond distance along the trajectories

As illustrated in Figure S7, the bond distance of H_2 exhibits notable oscillations over time, reflecting the stretching and compression caused by the energy released during its formation. The oscillations are particularly pronounced at position 2A, where more energy is retained by H_2. Initially, the bond undergoes high-amplitude oscillations, corresponding to the vibrationally excited state of the newly formed molecule. These fluctuations gradually diminish as energy is transferred to the graphene surface through vibrational coupling, leading to the relaxation of vibrational excitation at position 2A. In contrast, position C2 exhibits minimal oscillations and no noticeable relaxation.

We observe in figure S8 the two hydrogen atoms moving on the surface until they form H_2. Subsequently, the newly formed H_2 molecule begins to move away from the surface, continuing this trajectory until it reaches the boundary of our simulation cell. Beyond this point, the molecule interacts with an adjacent graphene sheet and begins to return toward the surface, an artifact of the simulation's boundary conditions. Therefore, our analysis focuses on the dynamics up to that point, ensuring that the interactions remain realistic.

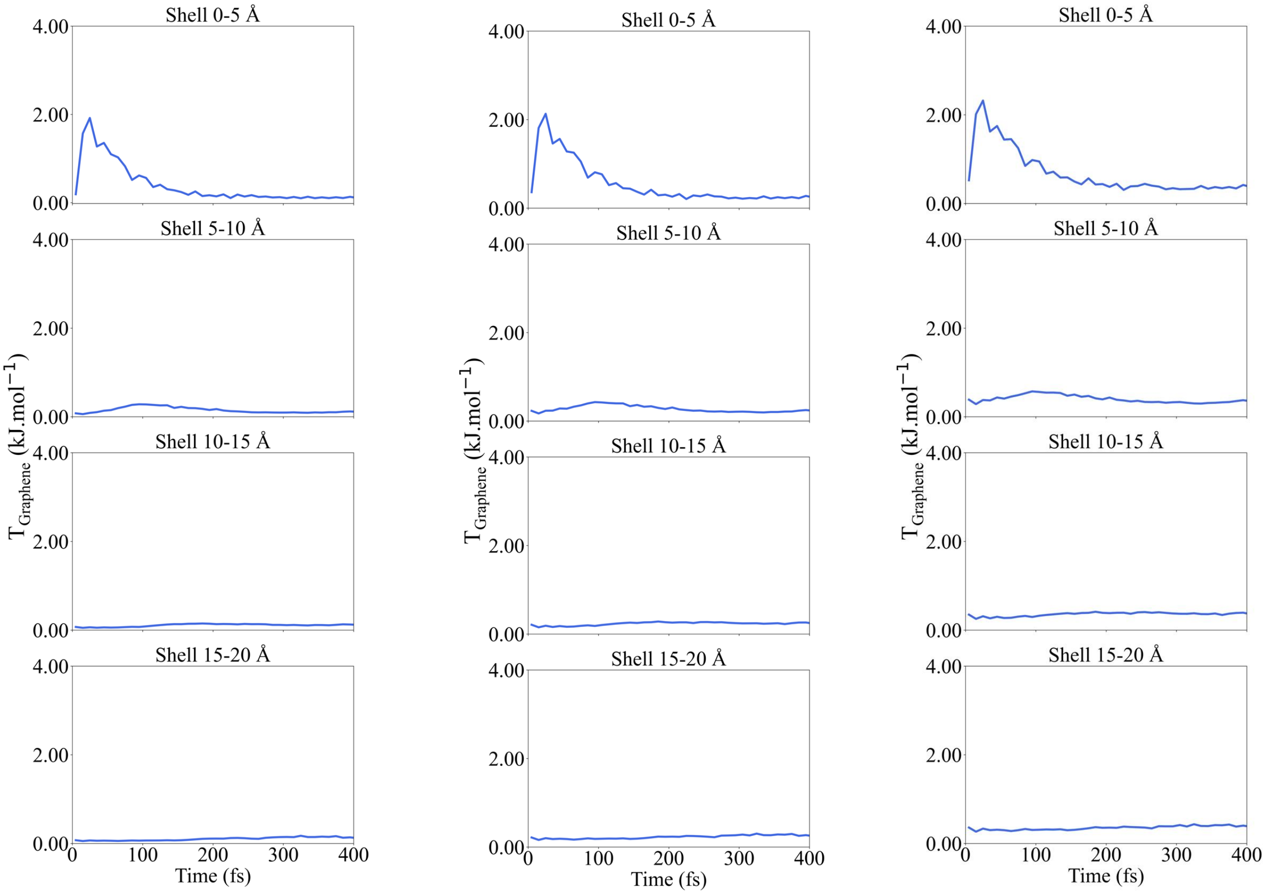

(d) PC at 10K (e) PC at 30K (f) PC at 50K

Fig. S5 Evolution of the averaged $T_{graphene}$ normalized per carbon atoms over 400 fs (in kJ mol^{-1}) in concentric shells centered at the H_2 formation reaction site in PC structure at the different temperatures.

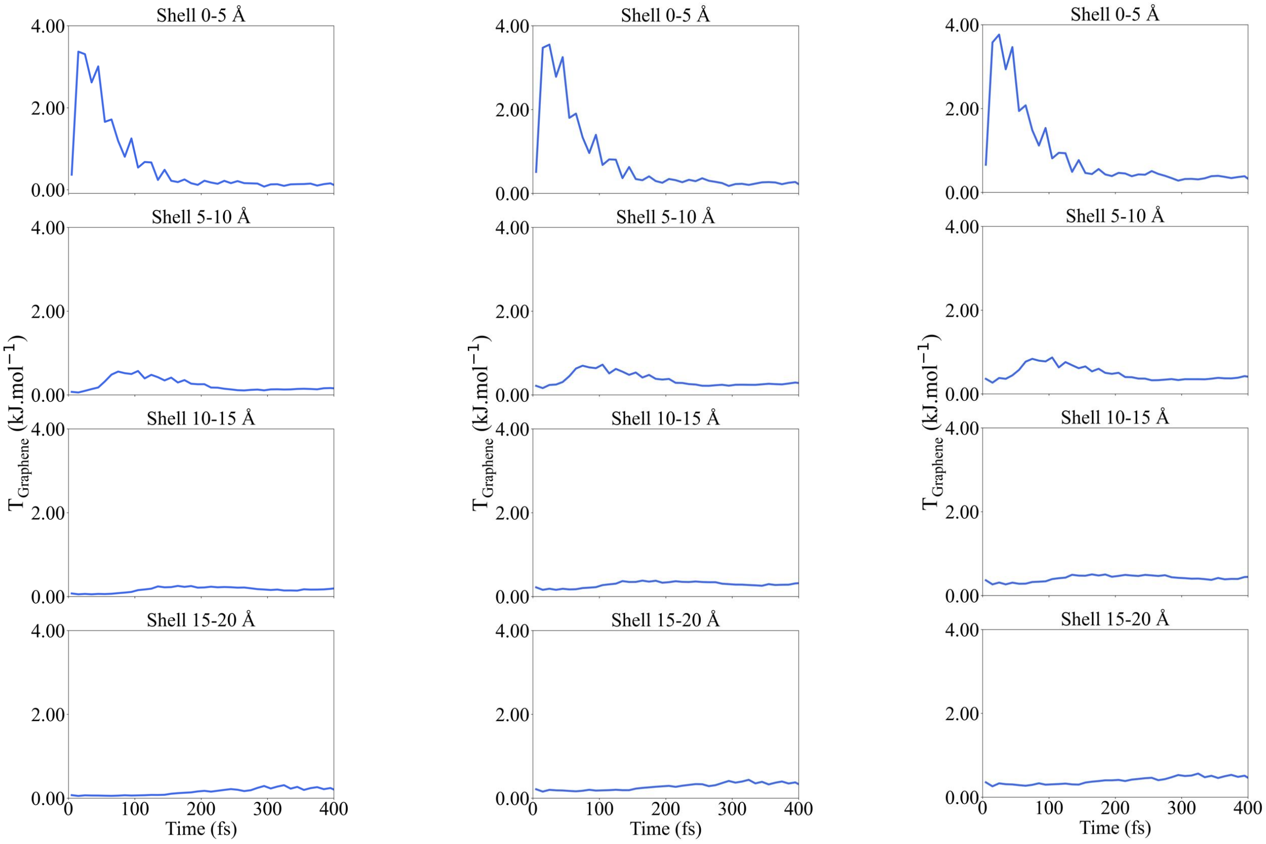

(g) CC at 10K

(h) CC at 30K

(i) CC at 50K

Fig. S6 Evolution of the averaged $T_{graphene}$ normalized per carbon atoms over 400 fs (in kJ mol^{-1}) in concentric shells centered at the H_2 formation reaction site in the CC structure at the different temperatures.

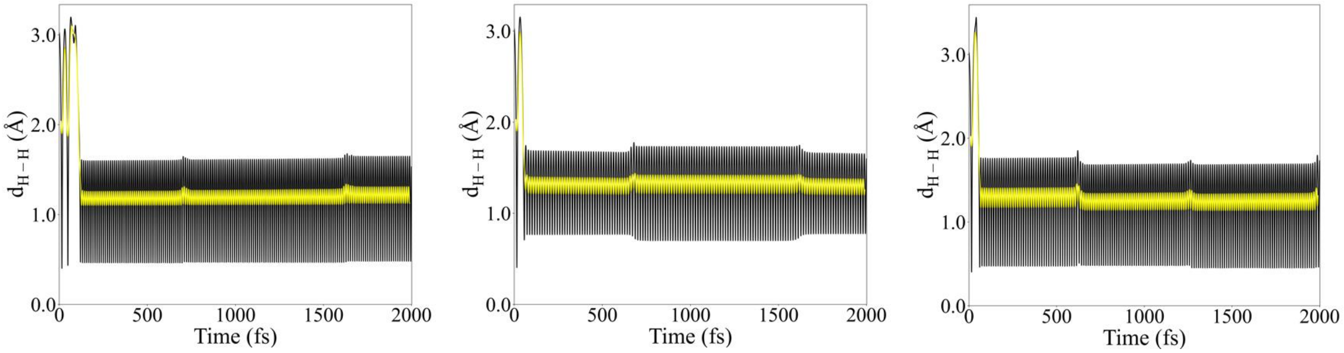

(a) PP at 10K

(b) PP at 30K

(c) PP at 50K

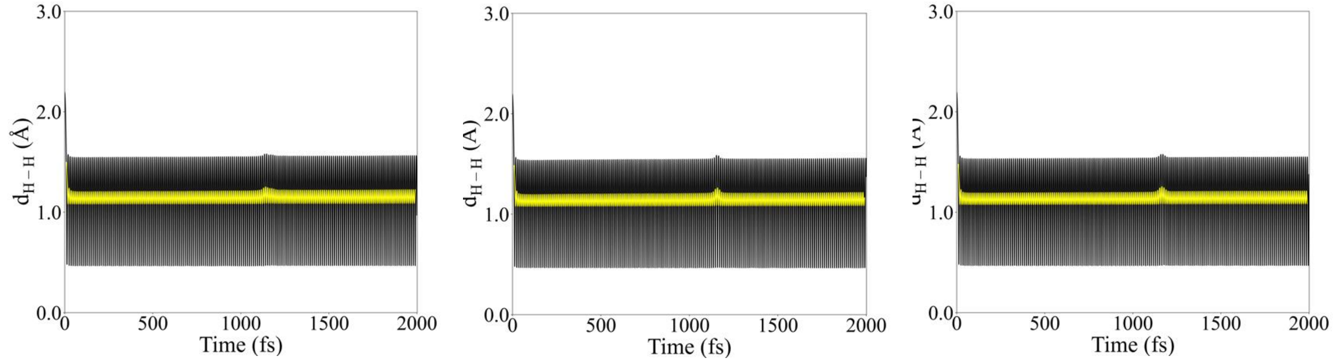

(d) PC at 10K

(e) PC at 30K

(f) PC at 50K

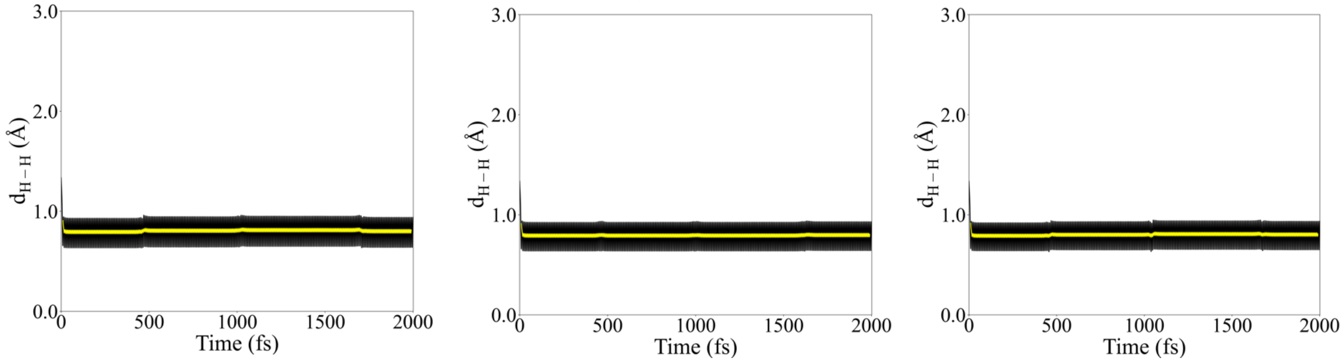

(g) CC at 10K

(h) CC at 30K

(i) CC at 50K

Fig. S7 Evolution of the H_2 bond distance over time in Å, with the moving average highlighted in yellow

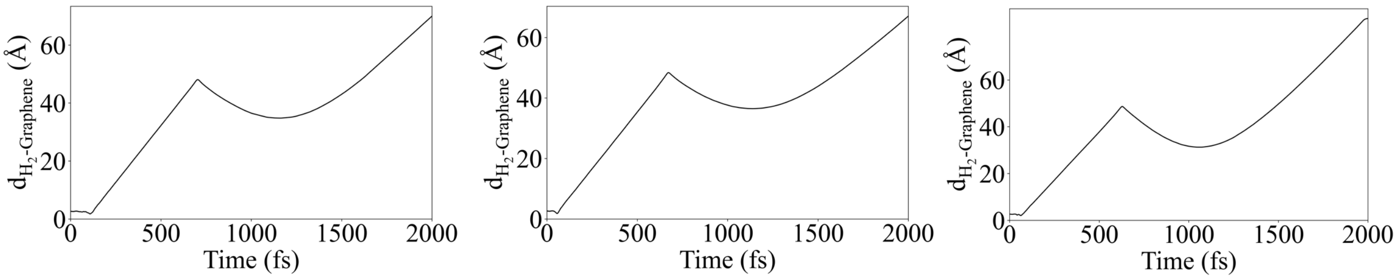

(a) PP at 10K

(b) PP at 30K

(c) PP at 50K

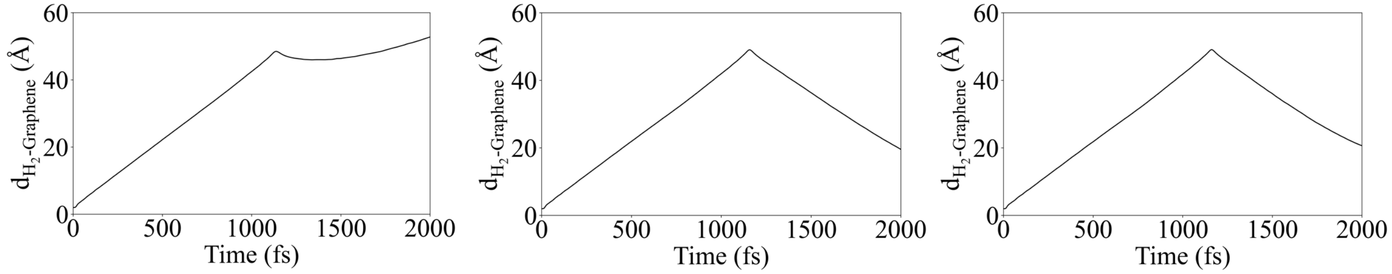

(d) PC at 10K

(e) PC at 30K

(f) PC at 50K

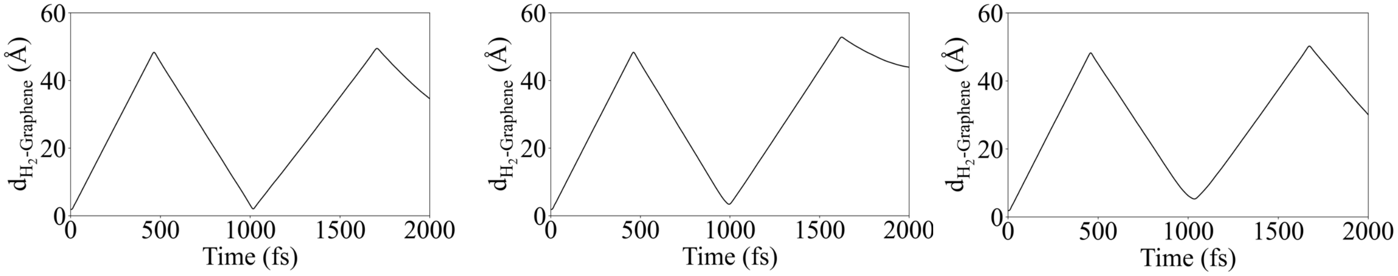

(g) CC at 10K

(h) CC at 30K

(i) CC at 50K

Fig. S8 Evolution of the Distance of H_2 from the Surface Over Time in Å